Initial Coupling and Reaction Progression of Directly Deposited Biradical Graphene Nanoribbon Monomers on Iodine-Passivated Versus Pristine Ag(111)

Gianluca Galeotti [1,†] , **Massimo Fritton** [1,2,†] , **Matthias Lischka** [1,2] , **Sebastian Obermann** [3] , **Ji Ma** [3] , **Wolfgang M. Heckl** [1,2] , **Xinliang Feng** [3,4] **and Markus Lackinger** [1,2,*]

1   Deutsches Museum, Museumsinsel 1, 80538 Munich, Germany; gianlucagaleotti86@gmail.com (G.G.); massimo.fritton@frm2.tum.de (M.F.); matthias.lischka@gmx.de (M.L.); generaldirektor@deutsches-museum.de (W.M.H.)
2   Department of Physics, Technische Universität München, James-Franck-Str. 1, 85748 Garching, Germany
3   Center for Advancing Electronics Dresden & Faculty of Chemistry and Food Chemistry, Technische Universität Dresden, 01069 Dresden, Germany; sebastian.obermann1@tu-dresden.de (S.O.); ji.ma@tu-dresden.de (J.M.); xinliang.feng@tu-dresden.de (X.F.)
4   Max Planck Institute of Microstructure Physics, Weinberg 2, 06120 Halle, Germany
*   Correspondence: markus@lackinger.org
†   These authors contributed equally to this work.

Abstract: The development of widely applicable methods for the synthesis of C-C-bonded nanostructures on inert and insulating surfaces is a challenging yet rewarding milestone in the field of on-surface synthesis. This would enable studies of nearly unperturbed covalent nanostructures with unique electronic properties as graphene nanoribbons (GNR) and π-conjugated 2D polymers. The prevalent Ullmann-type couplings are almost exclusively carried out on metal surfaces to lower the temperature required for initial dehalogenation well below the desorption threshold. To overcome the necessity for the activation of monomers on the target surface, we employ a recently developed Radical Deposition Source (RaDeS) for the direct deposition of radicals onto inert surfaces for subsequent coupling by addition reactions. The radicals are generated en route by indirect deposition of halogenated precursors through a heated reactive tube, where the dehalogenation reaction proceeds. Here, we use the ditopic 6,11-diiodo-1,2,3,4-tetraphenyltriphenylene (DITTP) precursor that afforded chevron-like GNR on Au(111) via the usual two-staged reaction comprised of monomer-coupling into covalent polymers and subsequent formation of an extended GNR by intramolecular cyclodehydrogenation (CDH). As a model system for inert surfaces, we use Ag(111) passivated with a closed monolayer of chemisorbed iodine that behaves in an inert manner with respect to dehalogenation reactions and facilitates the progressive coupling of radicals into extended covalent structures. We deposit the DITTP-derived biradicals onto both iodine-passivated and pristine Ag(111) surfaces. While on the passivated surface, we directly observe the formation of covalent polymers, on pristine Ag(111) organometallic intermediates emerge instead. This has decisive consequences for the further progression of the reaction: heating the organometallic chain directly on Ag(111) results in complete desorption, whereas the covalent polymer on iodine-passivated Ag(111) can be transformed into the GNR. Yet, the respective CDH proceeds directly on Ag(111) after thermal desorption of the iodine passivation. Accordingly, future work is aimed at the further development of approaches for the complete synthesis of GNR on inert surfaces.

Keywords: graphene nanoribbon; radical deposition; radical addition; inert surfaces; scanning tunneling microscopy

1. Introduction

Commonly referred to as a "wonder material" or the material of the future, graphene has been a thriving and inexhaustible topic in various branches of material research ever

since its first isolation by Geim and Novoselov in 2004 [1]. Graphene is expected to spark new fields of study and to revolutionize the industry [2,3] but its development does not come without challenges [4]. A commonly known downside is the lack of an electronic band gap, which is imperative for effective use in field-effect devices and transistors [5]. Even before the isolation of graphene, it was already known that quantum size effects, as implemented simply by structuring the 2D material into ribbons, are suitable for opening a bandgap [6]. Later, this was confirmed by the materialization of graphene nanoribbons (GNR) through distinct approaches such as wet-chemical synthesis [7], e-beam lithography [8], or the unzipping of carbon nanotubes [9]. These methods, however, facilitate only limited control over GNR width and edge termination, i.e., structural features that need to be controlled with atomic precision to obtain sufficiently uniform properties [10–13]. This demanding requirement led to the development of bottom-up fabrication methods on surfaces [14–16]. The established approach employs Ullmann-coupling of halogenated precursors on metal surfaces to afford covalent 1D polymers that are subsequently transformed into GNR by intramolecular cyclodehydrogenation (CDH) reactions. The Ullmann-coupling by itself is comprised of two main steps: first, the halogen substituents are dissociated with the aid of a reactive metal support, and second, intermolecular C-C bonds are formed by radical addition [17–19]. Depending on the type of metal and temperature, the reaction can directly proceed to completion [20] (commonly on Au) or metastable organometallic intermediates emerge (almost always on Cu and Ag). In many cases, these organometallic intermediates can be converted into covalent products by reductive elimination of the metal atom [21,22], but this can also fail [23,24] To induce the intramolecular CDH reactions that flatten the initial non-planar polymer into the GNR, further thermal activation at relatively high temperatures around 400 °C is required [25,26]. Thereby, DFT calculations also indicate a vital chemical contribution of the metal supports for the CDH and suggest a reaction progression in a domino-like fashion for the archetypal 7-armchair GNR [27].

While constraining the growth to two dimensions on surfaces is advantageous, the need for Ullmann-coupling limits the possible choice of surfaces mostly to metals. The chemical activity of metal supports lowers the reaction barrier for the initial dehalogenation so that it becomes feasible on the surface at temperatures before the reactants would desorb [28], although promising results were recently reported for TiO_2 surfaces [29]. Yet, projected GNR applications would benefit from a wide range of feasible supports also including semiconductor surfaces such as silicon [5]. Although protocols for the post-synthetic transfer from metals to alternative supports have been established [30,31], it remains challenging to avoid deterioration and contamination, thus synthesis on surfaces that are more relevant for applications is highly desirable. To realize C-C bond formation directly on inert and insulating surfaces, we recently developed a Radical Deposition Source (RaDeS) [32,33]. The conceptual idea is to deposit radicals rather than precursors in order to obviate the necessity of dehalogenation on the target surface. Thereby, the reaction step that requires metal surfaces is already carried out prior to deposition. Analogous to conventional Ullmann-couplings, halogenated precursors are used but deposited indirectly through a heated reactive tube, which constitutes the core piece of the RaDeS. There, halogen dissociation is activated either purely thermally in inert corundum tubes or with the aid of mildly reactive Au-coatings. The proof-of-concept for the direct deposition of radicals was demonstrated by depositing p-terphenyl biradicals generated en route from the respective iodinated precursor. On iodine-passivated Au(111), we first observed self-assembly of p-terphenyl or spontaneously dimerized p-sexiphenyl biradicals that progressively polymerized into extended poly-para-phenylene wires upon mild heating. Here, we employed 6,11-diiodo-1,2,3,4-tetraphenyltriphenylene (DITTP) molecules to extend our studies to more complex precursors and chemically active polymers. Both DITTP and its brominated analog were previously used as precursors for the synthesis of chevron-like GNR on Au(111) [14,34]. To shed light on the surface chemistry of directly deposited radicals on largely distinct supports, we compared iodine-passivated with pristine Ag(111) surfaces. In addition to room temperature (RT) deposition, we also studied the reaction

progression upon further heating on both types of surfaces. Thereby, we show that conventional synthesis of chevron-like GNR directly on Ag(111) is not feasible but requires the preceding formation of covalent polymers on the passivated surface.

2. Materials and Methods

All experiments were conducted under ultra-high vacuum (UHV) conditions with a base pressure below 3×10^{-10} mbar. Sample heating was performed with radiative heaters, and reported temperatures were measured with type K thermocouples mounted close to the sample. The Ag(111) single crystal (MaTeck) was prepared though repeated cycles of Ar$^+$-ion sputtering at 0.5 keV for 10 min followed by annealing at 490 °C for 15 min. The 6,11-diiodo-1,2,3,4-tetraphenyltriphenylene (DITTP) precursor was synthesized according to the reported procedure [35].

Freshly prepared Ag(111) crystals were iodine-passivated in a separate preparation chamber through exposure to 5×10^{-7} mbar of I$_2$ vapor for 10 min, followed by 15 min of annealing at 200 °C. Both the pristine and iodine-passivated Ag(111) surfaces were checked by STM imaging prior to deposition of molecules. Conventional deposition of DITTP was carried out with a home-built molecular evaporator [36]. Deposition of en route generated radicals was carried out with our RaDeS, which has been previously described in detail [32]. Prior to deposition with the RaDeS, its tube was cleaned and conditioned by in-vacuo heating to ~500 °C. For DITTP deposition via the RaDeS, a temperature of 200 °C . . . 220 °C was used for precursor sublimation, while the collector chamber that guides the molecules into the reactive tube was kept at a slightly higher temperature of ~230 °C. Two versions of the RaDeS were used equipped with either an inert corundum (Al$_2$O$_3$) tube or a mildly reactive gold-coated tube, operated at temperatures of >650 °C and 350 °C, respectively. Yet, the vastly different temperatures for the non-reactive versus reactive tube had no discernable impact on the observed structures.

STM images were acquired at room temperature in constant current mode, using a home-built instrument operated by a SPM 100 controller from RHK. Electrochemically etched tungsten tips were used, which were further conditioned in-situ by Ar$^+$-ion bombardment. The Gwyddion software was used for processing STM images by plane flattening and in some cases by using the correct horizontal scars and removing polynomial background functions (Figures 1a,c, 2b, 3b,c and S3–S5) [37].
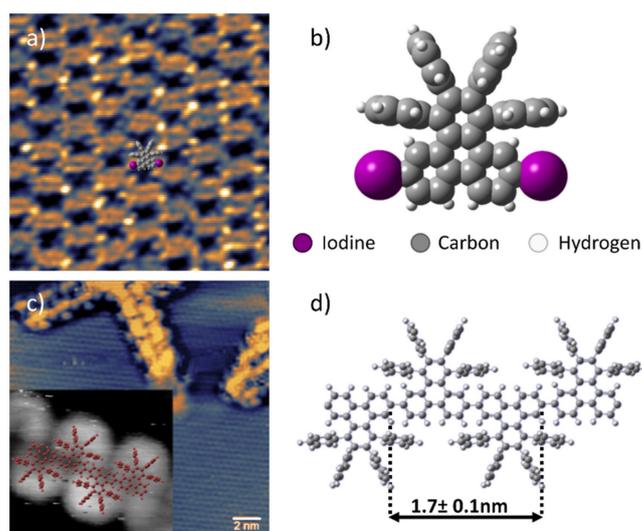
Figure 1. Conventional versus activated deposition. (**a**) STM image of DITTP conventionally deposited onto I-Ag(111) and (**b**) molecular structure of highly non-planar DITTP. (**c**) STM image of DITTP deposited onto I-Ag(111) via the RaDeS (the insert shows a close-up) and (**d**) corresponding model of the covalent polymer chain. Image parameters: (**a**): 11 × 11 nm², 93 pA, 1.13 V, pA, and 0 V; (**c**): 20 × 20 nm², 62 pA, and 2.5 V; and insert: 3 × 4 nm², 92 pA, and 2.7 V.
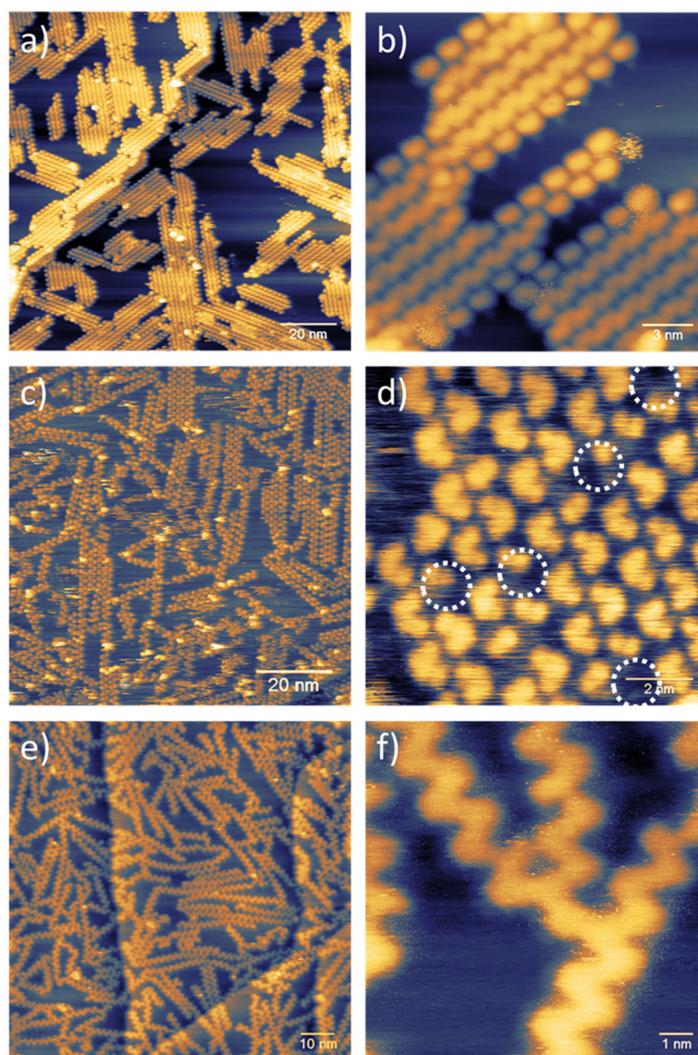
Figure 2. STM images of DITTP deposited onto I-Ag(111) via the RaDeS and annealed at increasing temperatures: (**a**,**b**) 200 °C, (**c**,**d**) 400 °C, and (**e**,**f**) 500 °C. The changes in packing and STM appearance of the chains are in accordance with a gradually progressing reaction from (**a**,**b**) covalent polymers to (**e**,**f**) GNR. Image parameters: (**a**): 120 × 120 nm^2, 90 pA, and 2.5 V; (**b**): 20 × 20 nm^2, 90 pA, and 2.5 V; (**c**): 90 × 90 nm^2, 88 pA, and 2.5 V; (**d**): 10 × 10 nm^2, 85 pA, and 2.5 V; (**e**): 100 × 100 nm^2, 92 pA, and 0.5 V; and (**f**): 10 × 10 nm^2, 92 pA, and 0.1 V.

To wet-chemically induce the CDH on the covalent polymers formed on iodine-passivated surfaces, we tried to generate a Scholl reaction in the solution. Therefore, we used iodine-passivated Au(111) (I-Au(111)) surfaces instead of I-Ag(111) as Au is more inert than Ag and high quality (111) films are available on mica (Georg-Albert-PVD). First, the covalent polymer was prepared on I-Au(111) in UHV by deposition with the RaDeS. Then, the sample was unloaded and immersed into a 50 mL single-neck round-bottom flask containing 20 mL of dry and degassed CH_2Cl_2 solution. Then the solution of $FeCl_3$ (100 mg) in 2.0 mL of nitromethane was added dropwise. After stirring at room temperature for 1 h under continuous argon bubbling, the sample was taken out, washed with methanol and further dried under vacuum. The sample was characterized by Raman spectroscopy at room temperature before and after the Scholl reaction (Figure S6) using a Renishaw inVia Raman spectrometer with an excitation wavelength of 532 nm.

The structure of the DITTP molecule was obtained using the MIT Atomic-Scale Modeling Toolkit available at NanoHub [38]. It uses GAMESS methods for DFT calculations,

with a B3LYP functional and the 6-311* basis set. Standard convergence criteria of the MIT Atomic-Scale Modeling Toolkit tool were applied.
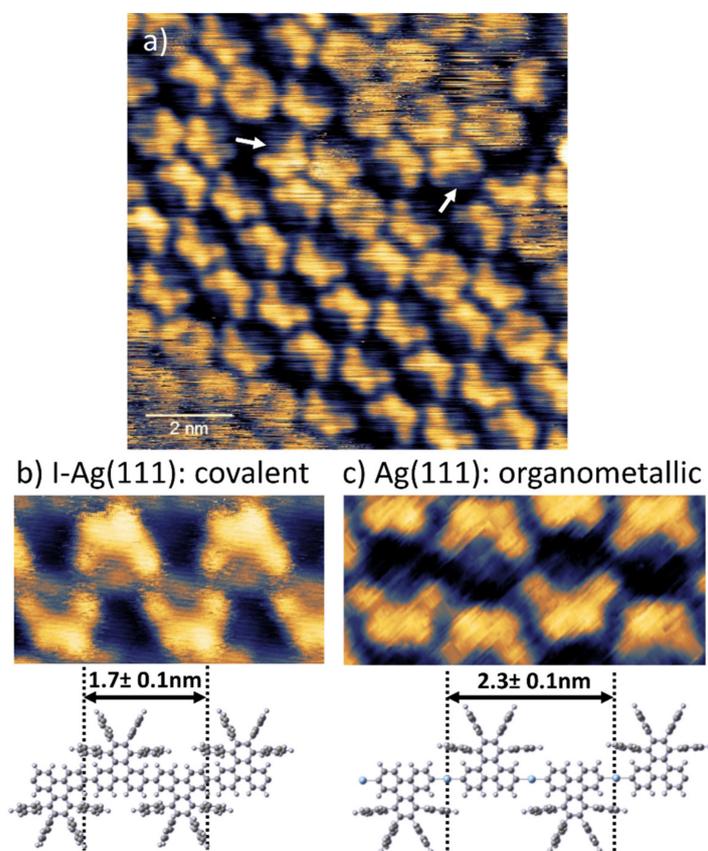
Figure 3. (**a**) STM image of organometallic chains and smaller entities observed upon deposition via the RaDeS onto pristine Ag(111). The white arrows highlight individual monomers. Comparison of both (**b**) covalent and (**c**) organometallic chains as obtained on I-Ag(111) and Ag(111), respectively. The corresponding molecular structures with their respective repeat distances are shown below. Image parameters: (**a**): 10×10 nm^2, 92 pA, and 0.3 V; (**b**): 89 pA and 1.45 V; and (**c**): 92 pA and 0.3 V.

3. Results

First, we studied the supramolecular self-assembly of the DITTP precursor on iodine-passivated Ag(111) (referred to as I-Ag(111) in the following) without preceding activation to evaluate the mobility of this relatively large and highly non-planar molecule on the highly corrugated chemisorbed iodine monolayer. Conventional deposition of DITTP by thermal sublimation results in the self-assembly of intact molecules and a representative STM image is shown in Figure 1a. The structure features a nearly hexagonal lattice with a = b = 1.6 ± 0.1 nm, γ = 123° ± 5°, and bears strong resemblance to that reported for the brominated analog on Au(111) by Bronner et al. [34]. Yet, on I-Ag(111), self-assembly is observed directly after RT deposition, while on Au(111), mild heating to 50 °C was required to promote the ordering process. This already reflects the higher mobility on the passivated I-Ag(111) as compared to the bare Au(111) metal surface. Nevertheless, self-assembly of similar structures on these very distinct supports insinuates the dominance of molecule–molecule interactions (cf. Figure S1 for details of the supramolecular ordering). Even though the self-assembled structures of this precursor on Au(111) and I-Ag(111) are similar, their further progression upon heating could not be any more different. On Au(111), the expected Ullmann-coupling into a covalent polymer was observed [34], whereas the heating of DITP on I-Ag(111) to 200 °C merely resulted in desorption, yielding a clean surface (Figure S2). This corroborates the inertness of iodine-passivated metals with respect to dehalogenation reactions [32]. We presume that the relatively low desorption temperature

of DITTP that lies in the range of the sublimation temperature is a consequence of both its highly non-planar structure caused by the steric hindrance of the phenyl substituents (Figure 1b) and the general weakness of molecule–surface interactions on iodine-passivated surfaces [39,40].

In contrast, deposition of activated, i.e., dehalogenated, DITTP onto I-Ag(111) using our RaDeS results in polymer chains adsorbed on the clearly visible $\sqrt{3} \times \sqrt{3} \, R30°$ iodine superstructure (Figure 1c). These are comprised of crescent-shaped features with alternating orientations along the chain. The measured repeat distance amounts to 1.7 ± 0.1 nm. Despite obvious differences in the STM appearance of the short chains, their repeat distance is always similar, suggesting identical chemical structures. We propose that the deposition of the DITTP-derived biradicals results in the direct formation of covalent chains (Figure 1d). As illustrated by the overlay, the crescents correspond to an envelope of the phenyl substituents, which are rotated out of plane due to steric hindrance in accordance with other oligophenylene precursors [41]. The alternating orientation of the crescents results from the pronounced intermolecular steric hindrance, which precludes covalent-coupling of similarly oriented molecules [14]. This structural assignment is corroborated by the agreement of both the STM contrast as well as the chain periodicity to previous experimental and theoretical results for the analogous covalent chains on Au(111) [14,34]. Acquiring STM images of the as-prepared sample at RT was challenging and required relatively low setpoint currents. The situation improved after mild annealing to 200 °C probably due to merging of short chains into longer, better stabilized ones, an observation in accordance with our previous study of terphenyl biradicals on I-Ag(111) [32]. We did not observe evident differences in the formed structures using a RaDeS with an inert corundum or Au-coated tube.

To further study structural and/or chemical changes induced by thermal activation, the sample was first heated to 200 °C. The STM images in Figure 2a,b show the reorganization of the polymer chains into aligned domains. Both the periodicity and STM contrast of the chains remained unaffected, suggesting that no chemical changes had occurred. The chain axes were oriented 30° with respect to the high symmetry direction of the iodine monolayer (i.e., along the high symmetry direction of Au(111)) and, accordingly, three distinct domain orientations were found. Adjacent chains were shifted by half the repeat distance to allow for a favorable packing (Figure S3). DFT calculations of the brominated analog suggest that this packing was driven by interactions between the phenyl substituents [14]. The distance between adjacent chains amounts to 1.7 ± 0.1 nm on average (Figure S3). Moreover, we observed clear differences in the STM contrast of the chains between the interior and exterior of the domains (Figure S3), where the crescents appear smeared out at the rim. Various reasons could account for these contrast differences, including relaxation effects and even STM imaging characteristics, but the most plausible explanation relates to an enhanced freedom of movement of the phenyl substituents, with the possibility to orient toward the substrate (Figure S3). Such a propeller-like conformation is common for analogous molecules with terminal phenyls [41]. The average length of the covalent chains amounts to ~25 nm, with individual lengths ranging from as short as 10 nm up to > 60 nm, while the aggregate sizes range from occasionally observed single chains up to domains of >15 chains.

After further heating to relatively high temperatures of 400 °C, the polymer chains were still observed on the surface, clearly indicating their high stability in line with the proposed covalent bonding. Yet, this thermal treatment resulted in evident changes (Figure 2c,d). Instead of being organized into condensed domains, the polymer chains were then dispersed across the surface without any apparent orientational ordering. We did not observe a significant change in the length distribution of the chains, suggesting that this additional heating does not result in further covalent-coupling. Presumably, these long chains do not possess the necessary mobility and maneuverability, but we can also not exclude passivation of the terminal radical sites by hydrogen. The iodine passivation layer was not detectable by STM anymore due to thermal desorption. The desorption

temperature was in the expected range, albeit complete desorption of the iodine monolayer requires around 500 °C [42,43]. As a consequence of the iodine desorption, the covalent polymers became directly adsorbed on the bare metal surface, as similarly observed for the reversible iodine intercalation between 2D polymers and their Au(111) support [44]. Aligned chains could still be found but on bare Ag(111), the interchain distance increased markedly to 2.3 nm (Figure S4) as compared to the 1.7 nm found for I-Ag(111). This increased spacing hints at a stronger interaction with the metal surface, where more flat adsorbed phenyl moieties require more space. Despite the increased interchain spacing, there was still an offset of a half-repeat distance between adjacent chains, indicating the prevalence of a related packing motif. More importantly, in the STM contrast, the separated crescent features remained mostly unchanged, suggesting the absence of overall chemical changes despite the relatively high annealing temperature. Interestingly, the different STM contrast at the domain edge as observed on I-Ag(111) (vide supra) also disappeared, suggesting an overriding influence of stronger molecule–surface interactions directly on Ag(111). Some chains exhibited point defects in their STM appearance, where the normally bright-appearing crescent feature was completely or partially missing (white dotted circles in Figure 2d). We interpret this contrast change as a signature of the first CDH reactions that eventually transform the polymer into the GNR. The resulting more planar structure is in accordance with the lower apparent height in STM. Interestingly, local occurrence of the CDH apparently contradicts previous theoretical work that proposed a zipping mechanism for the 7-armchair GNR, where an initial CDH results in a propagating reaction along the polymers [27]. Yet, in the 7-armchair GNR, the CDH at one site had a stronger effect on the adjacent site, whereas for the chevron-like GNR, here, the CDH on adjacent sites should affect each other significantly less.

Heating at 500 °C results in completion of the CDH. As shown in Figure 2e,f, the thereby attained GNR appears completely flat in STM with a uniform height and without internal features, as expected for extended aromatic structures directly adsorbed on metals. The GNR did not show a preferred orientation anymore and often exhibited a slight curvature instead of the expected straight-line shape. Moreover, we did not find a preferred packing motif between adjacent GNR anymore. In addition, we observed junctions without a separating gap between the individual GNR (Figure 2f), suggesting covalent merging. The lateral fusion of adjacent GNR chains is well known and was exploited for the synthesis of 2D polymers [45].

Yet, the complete synthesis of GNR on passivated surfaces still remains the overarching goal. As a proof-of-principle, we attempted to induce the CDH on the passivated surface by wet-chemical means. Therefore, covalent polymers were prepared on I-Au(111) and exposed to a $FeCl_3$ containing solution under Schlenk conditions to induce the Scholl reaction. Albeit Raman spectroscopy indicates successful GNR formation on the surface (Figure S6), subsequent STM imaging was not possible due to persistent contaminations. Moreover, the iodine monolayer might not withstand this relatively harsh chemistry, indicating the need for chemically more robust substrates.

While we achieved GNR formation on Ag(111) starting from the covalent polymer on I-Ag(111), we wanted to further explore the coupling of directly deposited radicals on pristine rather than on passivated Ag(111). To this end, we employed the RaDeS to directly deposit the biradicals on bare Ag(111) using similar deposition parameters as before. In the same manner, STM images show the immediate formation of chains, yet with a markedly increased repeat distance of 2.3 nm. This is about 0.6 nm longer as compared to the covalent chains formed directly on I-Ag(111) (Figure 3 and Figure S5). This increase indicates the formation of organometallic rather than covalent chains, where monomers are linked via C-Ag-C bonds. Since the repeat unit here was comprised of two molecules, each intermolecular bond was about 0.3 nm longer than the respective covalent bond, a difference that is in accordance with the literature [22,40,42,46]. Moreover, the increased repeat distance allows for tighter packing of the chains, resulting in a decreased interchain

distance of 1.4 ± 0.1 nm as compared to 1.7 nm for the covalent chains on I-Ag(111) (Figure S5).

Recent measurements of the adsorption height of the binding organometallic carbon atoms by X-ray standing waves made a strong case for the Ag atoms being adatoms rather than surface atoms [40,46]. This is also in accordance with their bright STM appearance [42]. Here, the Ag atoms were completely outshined by the phenyl substituents. Additionally, in the organometallic chains, the orientation of the monomers alternated along the chains as the increased length of the organometallic bond was still not sufficient to remove the steric hindrance for binding between identically oriented monomers. Yet, we presume that both the increased repeat distance in the organometallic chains and the stronger interactions with the pristine Ag(111) surface result in more planar adsorption of the phenyl substituents and concomitant changes in both their width and STM appearance. Moreover, the enhanced interaction with the surface also had its bearing on structure formation on pristine Ag(111): remarkably, as shown in Figure 3a, we often observed smaller organometallic entities, i.e., single molecules (marked by white arrows in Figure 3a), short fragments, and highly bent linkages, all of which were not present in the covalent chains on I-Ag(111). We interpret this as evidence for restricted monomer mobility on pristine Ag(111) as compared to the iodine-passivated surface. Moreover, the higher bond angle flexibility of the organometallic linkages facilitates adaptations [23].

We also studied the reaction progression of the organometallic chains upon further heating. Interestingly, conversion to covalent chains by the reductive elimination of the organometallic Ag atoms turned out to be unfeasible. STM images acquired after sample heating to 200 °C just showed an empty Ag(111) surface, indicating full desorption of the organometallic structures. We reason that the highly non-planar molecular structure with the tilted phenyl substituents also increases the overall adsorption height of the triphenylene scaffold, which is expected to weaken both the strength of the organometallic bond to the low-lying Ag adatom and the cohesion to Ag(111). The conversion of organometallic to covalent can be associated with relatively high energy barriers in the order of ~1 . . . 2 eV as suggested by DFT calculations [47]. This manifests experimentally in conversion temperatures around 150 °C as experimentally determined by STM and temperature-programmed X-ray photoelectron spectroscopy studies [42,48]. It is reasonable to presume, thus, a not systematically well-explored influence of the molecular structure on both reaction barriers and temperatures that can arise from steric hindrance or molecule–surface interactions. For instance, desorption rather than conversion of organometallic intermediates to covalent products was likewise observed for the 1-1' linking between pyrenes [24]. In particular, constraining the reaction to a planar venue (as at least partly imposed by interactions with the surface) considerably increases the energy barrier for conversion. For too high reaction barriers, heating will result in desorption of the organometallic structures rather than in their conversion. At this point, it remains unclear whether the molecules directly desorb from the organometallic structure or whether the chains disintegrate first and then isolated molecules desorb from Ag(111).

4. Discussion and Summary

In summary, we demonstrated the synthesis of covalently linked polymer chains from DITTP precursor molecules on iodine-passivated Ag(111) by means of depositing en route-generated biradicals. Direct formation of polymer chains indicates sufficient monomer mobility, yet further mild heating at 200 °C resulted in extended covalent chains up to a length of 60 nm. This confirms that the preformed oligomers still remain active for progressive covalent-coupling. In other words, the bonds formed between radical sites and iodine atoms in the passivation layer are dynamic in nature.

Deposition of the biradicals directly onto pristine Ag(111) unveiled interesting principal differences. Instead of covalent chains, we observed the formation of short organometallic segments. This indicates low mobility of the radicals on the bare metal surface at room temperature, as similarly suggested by experiments with ultraviolet light-induced dehalo-

genation [49]. This may also explain formation of organometallic intermediates rather than the covalent products, where bonding with Ag atoms provided by the free adatom gas is kinetically preferred. Interestingly, the conversion of the organometallic into covalent polymers directly on Ag(111) was not possible and heating just resulted in desorption. The most likely reason is an increase of the reaction barrier due to steric hindrance between the bulky phenyl substituents in combination with weakened molecule–surface bonds due to the highly non-planar structure.

Similarly, conversion of the covalent polymer by thermal activation of the CDH directly on I-Ag(111) is not feasible because the iodine passivation layer is no longer stable at the required relatively high reaction temperatures. Yet, the covalent polymer becomes directly adsorbed on Ag(111), where the CDH readily proceeds. The observation of single CDH events precludes a zipping mechanism for the chevron-like GNR. Unfortunately, the limited thermal stability of the iodine passivation layer leaves the interesting question of the feasibility of a purely thermal CDH unaddressed. Nevertheless, the protocol based on the prior formation of the covalent structure on a passivated metal and carrying out the final reaction step on the metal after de-passivation facilitates GNR synthesis on Ag(111). By contrast, direct synthesis of the chevron-like GNR on Ag(111) remains elusive within the conventional approach. In addition, we provide the first evidence that CDH can also be induced on surfaces wet-chemically by the established Scholl reaction, albeit the STM characterization was not possible. To this end, more inert substrates may offer the possibility for high-resolution imaging also after the harsh wet-chemical treatment. Alternatively, replacing the CDH by cyclodehalohydrogenations, where HX (X being a stronger-bound halogen such as Cl or F) is eliminated instead of H_2, has proven to be a viable means to realize lower reaction temperatures by lowering reaction barriers [29]. Consequently, it would be highly interesting to study chemically modified precursors with our approach for the complete synthesis of GNR on iodine-passivated metals. Additional advanced possibilities for synthesis by direct deposition of radicals that reach beyond the established pathways on metal surfaces could be gained by changing the substrate, for instance, by using more anisotropic surfaces to imprint a growth direction as well as patterning of the passivation layer or by tuning its reactivity.

Supplementary Materials: The following supporting information can be downloaded at: https://www.mdpi.com/article/10.3390/chemistry4020020/s1, Figures S1–S5: Additional STM data, Figure S6: Raman characterization before and after the Scholl reaction. References [50–55] are cited in the Supplementary Materials.

Author Contributions: M.L. (Markus Lackinger), X.F. and W.M.H. conceived, designed, and supervised the study. G.G., M.F. and M.L. (Matthias Lischka) carried out the experimental work including the sample preparation and STM experiments. G.G. analyzed the data and performed the simulations. S.O. and J.M. synthesized the DITTP compound and carried out the Scholl reaction in solution. G.G. and M.L. (Markus Lackinger) co-wrote the manuscript with contributions from all co-authors. All authors have read and agreed to the published version of the manuscript.

Funding: This research was funded by the Deutsche Forschungsgemeinschaft grant number LA 1842/9-1.

Data Availability Statement: All necessary data are presented in the manuscript and the Supplementary Materials. Additional data are available from the corresponding author upon reasonable request.

Acknowledgments: We gratefully acknowledge funding by the Deutsche Forschungsgemeinschaft (DFG) grant LA 1842/9-1.

Conflicts of Interest: The authors declare no competing interests.

References

1. Novoselov, K.S.; Geim, A.K.; Morozov, S.V.; Jiang, D.; Zhang, Y.; Dubonos, S.V.; Grigorieva, I.V.; Firsov, A.A. Electric Field Effect in Atomically Thin Carbon Films. *Science* **2004**, *306*, 666–669. [CrossRef] [PubMed]
2. Bonaccorso, F.; Sun, Z.; Hasan, T.; Ferrari, A.C. Graphene photonics and optoelectronics. *Nat. Photon.* **2010**, *4*, 611–622. [CrossRef]
3. Geim, A.K. Graphene: Status and Prospects. *Science* **2009**, *324*, 1530–1534. [CrossRef] [PubMed]

4. Kong, W.; Kum, H.; Bae, S.-H.; Shim, J.; Kim, H.; Kong, L.; Meng, Y.; Wang, K.; Kim, C.; Kim, J. Path towards graphene commercialization from lab to market. *Nat. Nano.* **2019**, *14*, 927–938. [CrossRef]

5. Schwierz, F. Graphene transistors. *Nat. Nanotechnol.* **2010**, *5*, 487–496. [CrossRef]

6. Nakada, K.; Fujita, M.; Dresselhaus, G.; Dresselhaus, M.S. Edge state in graphene ribbons: Nanometer size effect and edge shape dependence. *Phys. Rev. B* **1996**, *54*, 17954–17961. [CrossRef]

7. Li, X.; Wang, X.; Zhang, L.; Lee, S.; Dai, H. Chemically Derived, Ultrasmooth Graphene Nanoribbon Semiconductors. *Science* **2008**, *319*, 1229–1232. [CrossRef]

8. Han, M.Y.; Özyilmaz, B.; Zhang, Y.; Kim, P. Energy Band-Gap Engineering of Graphene Nanoribbons. *Phys. Rev. Lett.* **2007**, *98*, 206805. [CrossRef]

9. Kosynkin, D.V.; Higginbotham, A.L.; Sinitskii, A.; Lomeda, J.R.; Dimiev, A.; Price, B.K.; Tour, J.M. Longitudinal unzipping of carbon nanotubes to form graphene nanoribbons. *Nature* **2009**, *458*, 872–876. [CrossRef]

10. Son, Y.-W.; Cohen, M.L.; Louie, S.G. Energy Gaps in Graphene Nanoribbons. *Phys. Rev. Lett.* **2006**, *97*, 216803. [CrossRef]

11. Barone, V.; Hod, O.; Scuseria, G.E. Electronic Structure and Stability of Semiconducting Graphene Nanoribbons. *Nano Lett.* **2006**, *6*, 2748–2754. [CrossRef] [PubMed]

12. Yoon, Y.; Guo, J. Effect of edge roughness in graphene nanoribbon transistors. *Appl. Phys. Lett.* **2007**, *91*, 073103. [CrossRef]

13. Houtsma, R.S.K.; de la Rie, J.; Stöhr, M. Atomically precise graphene nanoribbons: Interplay of structural and electronic properties. *Chem. Soc. Rev.* **2021**, *50*, 6541–6568. [CrossRef] [PubMed]

14. Cai, J.; Ruffieux, P.; Jaafar, R.; Bieri, M.; Braun, T.; Blankenburg, S.; Muoth, M.; Seitsonen, A.P.; Saleh, M.; Feng, X. Atomically precise bottom-up fabrication of graphene nanoribbons. *Nature* **2010**, *466*, 470–473. [CrossRef] [PubMed]

15. Ruffieux, P.; Wang, S.; Yang, B.; Sánchez-Sánchez, C.; Liu, J.; Dienel, T.; Talirz, L.; Shinde, P.; Pignedoli, C.A.; Passerone, D.; et al. On-surface synthesis of graphene nanoribbons with zigzag edge topology. *Nature* **2016**, *531*, 489–492. [CrossRef] [PubMed]

16. Talirz, L.; Ruffieux, P.; Fasel, R. On-Surface Synthesis of Atomically Precise Graphene Nanoribbons. *Adv. Mater.* **2016**, *28*, 6222–6231. [CrossRef]

17. Lipton-Duffin, J.A.; Miwa, J.A.; Kondratenko, M.; Cicoira, F.; Sumpter, B.G.; Meunier, V.; Perepichka, D.F.; Rosei, F. Step-by-step growth of epitaxially aligned polythiophene by surface-confined reaction. *Proc. Natl. Acad. Sci. USA* **2010**, *107*, 11200–11204. [CrossRef]

18. Blake, M.M.; Nanayakkara, S.U.; Claridge, S.A.; Fernández-Torres, L.C.; Sykes, E.C.H.; Weiss, P.S. Identifying Reactive Intermediates in the Ullmann Coupling Reaction by Scanning Tunneling Microscopy and Spectroscopy. *J. Phys. Chem. A* **2009**, *113*, 13167–13172. [CrossRef]

19. Xi, M.; Bent, B.E. Mechanisms of the Ullmann coupling reaction in adsorbed monolayers. *J. Am. Chem. Soc.* **1993**, *115*, 7426–7433. [CrossRef]

20. Grill, L.; Dyer, M.; Lafferentz, L.; Persson, M.; Peters, M.V.; Hecht, S. Nano-architectures by Covalent Assembly of Molecular Building Blocks. *Nat. Nanotechnol.* **2007**, *2*, 687. [CrossRef]

21. Di Giovannantonio, M.; El Garah, M.; Lipton-Duffin, J.; Meunier, V.; Cardenas, L.; Fagot Revurat, Y.; Cossaro, A.; Verdini, A.; Perepichka, D.F.; Rosei, F.; et al. Insight into Organometallic Intermediate and Its Evolution to Covalent Bonding in Surface-Confined Ullmann Polymerization. *ACS Nano* **2013**, *7*, 8190–8198. [CrossRef] [PubMed]

22. Eichhorn, J.; Strunskus, T.; Rastgoo-Lahrood, A.; Samanta, D.; Schmittel, M.; Lackinger, M. On-surface Ullmann polymerization via intermediate organometallic networks on Ag(111). *Chem. Commun.* **2014**, *50*, 7680–7682. [CrossRef] [PubMed]

23. Fritton, M.; Otte, K.; Björk, J.; Biswas, P.K.; Heckl, W.M.; Schmittel, M.; Lackinger, M. The influence of ortho-methyl substitution in organometallic self-assembly—A comparative study on Cu(111) vs. Ag(111). *Chem. Commun.* **2018**, *54*, 9745–9748. [CrossRef] [PubMed]

24. Lischka, M.; Fritton, M.; Eichhorn, J.; Vyas, V.S.; Strunskus, T.; Lotsch, B.V.; Björk, J.; Heckl, W.M.; Lackinger, M. On-Surface Polymerization of 1,6-Dibromo-3,8-diiodpyrene—A Comparative Study on Au(111) Versus Ag(111) by STM, XPS, and NEXAFS. *J. Phys. Chem. C* **2018**, *122*, 5967–5977. [CrossRef]

25. Sánchez-Sánchez, C.; Brüller, S.; Sachdev, H.; Müllen, K.; Krieg, M.; Bettinger, H.F.; Nicolaï, A.; Meunier, V.; Talirz, L.; Fasel, R.; et al. On-Surface Synthesis of BN-Substituted Heteroaromatic Networks. *ACS Nano* **2015**, *9*, 9228–9235. [CrossRef]

26. Massimi, L.; Ourdjini, O.; Lafferentz, L.; Koch, M.; Grill, L.; Cavaliere, E.; Gavioli, L.; Cardoso, C.; Prezzi, D.; Molinari, E.; et al. Surface-Assisted Reactions toward Formation of Graphene Nanoribbons on Au(110) Surface. *J. Phys. Chem. C* **2015**, *119*, 2427–2437. [CrossRef]

27. Björk, J.; Stafström, S.; Hanke, F. Zipping Up: Cooperativity Drives the Synthesis of Graphene Nanoribbons. *J. Am. Chem. Soc.* **2011**, *133*, 14884–14887. [CrossRef]

28. Lackinger, M. Surface-assisted Ullmann coupling. *Chem. Commun.* **2017**, *53*, 7872–7885. [CrossRef]

29. Kolmer, M.; Steiner, A.K.; Izydorczyk, I.; Ko, W.; Engelund, M.; Szymonski, M.; Li, A.-P.; Amsharov, K. Rational synthesis of atomically precise graphene nanoribbons directly on metal oxide surfaces. *Science* **2020**, *369*, 571–575. [CrossRef]

30. Llinas, J.P.; Fairbrother, A.; Borin Barin, G.; Shi, W.; Lee, K.; Wu, S.; Yong Choi, B.; Braganza, R.; Lear, J.; Kau, N.; et al. Short-channel field-effect transistors with 9-atom and 13-atom wide graphene nanoribbons. *Nat. Commun.* **2017**, *8*, 633. [CrossRef]

31. Borin Barin, G.; Fairbrother, A.; Rotach, L.; Bayle, M.; Paillet, M.; Liang, L.; Meunier, V.; Hauert, R.; Dumslaff, T.; Narita, A.; et al. Surface-Synthesized Graphene Nanoribbons for Room Temperature Switching Devices: Substrate Transfer and ex Situ Characterization. *ACS Appl. Nano Mater.* **2019**, *2*, 2184–2192. [CrossRef]

32. Galeotti, G.; Fritton, M.; Lackinger, M. Carbon-Carbon Coupling on Inert Surfaces by Deposition of En Route Generated Aryl Radicals. *Angew. Chem. Int. Ed.* **2020**, *59*, 22785–22789. [CrossRef] [PubMed]

33. Lackinger, M. Synthesis on inert surfaces. *Dalton T* **2021**, *50*, 10020–10027. [CrossRef] [PubMed]

34. Bronner, C.; Marangoni, T.; Rizzo, D.J.; Durr, R.A.; Jørgensen, J.H.; Fischer, F.R.; Crommie, M.F. Iodine versus Bromine Functional-ization for Bottom-Up Graphene Nanoribbon Growth: Role of Diffusion. *J. Phys. Chem. C* **2017**, *121*, 18490–18495. [CrossRef]

35. Thiessen, A.; Wettach, H.; Meerholz, K.; Neese, F.; Hoger, S.; Hertel, D. Control of electronic properties of triphenylene by substitution. *Org. Electron.* **2012**, *13*, 71–83. [CrossRef]

36. Gutzler, R.; Heckl, W.M.; Lackinger, M. Combination of a Knudsen effusion cell with a quartz crystal microbalance: In situ measurement of molecular evaporation rates with a fully functional deposition source. *Rev. Sci. Instrum.* **2010**, *81*, 015108. [CrossRef]

37. Nečas, D.; Klapetek, P. Gwyddion: An open-source software for SPM data analysis. *Open Phys.* **2012**, *10*, 181–188. [CrossRef]

38. Richards, D.; Ertekin, E.; Grossman, J.C.; Strubbe, D.; Riley, J.; Guerrero, E. MIT Atomic-Scale Modeling Toolkit. 2021. Available online: https://nanohub.org/resources/ucb_compnano (accessed on 1 March 2022).

39. Rastgoo-Lahrood, A.; Björk, J.; Lischka, M.; Eichhorn, J.; Kloft, S.; Fritton, M.; Strunskus, T.; Samanta, D.; Schmittel, M.; Heckl, W.M.; et al. Post-Synthetic Decoupling of On-Surface-Synthesized Covalent Nanostructures from Ag(111). *Angew. Chem. Int. Ed.* **2016**, *55*, 7650–7654. [CrossRef]

40. Grossmann, L.; Duncan, D.A.; Jarvis, S.P.; Jones, R.G.; De, S.; Rosen, J.; Schmittel, M.; Heckl, W.M.; Björk, J.; Lackinger, M. Evolution of adsorption heights in the on-surface synthesis and decoupling of covalent organic networks on Ag(111) by normal-incidence X-ray standing wave. *Nanoscale Horiz.* **2022**, *7*, 51–62. [CrossRef]

41. Gust, D. Restricted rotation in hexaarylbenzenes. *J. Am. Chem. Soc.* **1977**, *99*, 6980–6982. [CrossRef]

42. Galeotti, G.; De Marchi, F.; Taerum, T.; Besteiro, L.; El Garah, M.; Lipton-Duffin, J.; Ebrahimi, M.; Perepichka, D.; Rosei, F. Surface-mediated Assembly, Polymerization and Degradation of Thiophene-based Monomers. *Chem. Sci.* **2019**, *10*, 5167–5175. [CrossRef] [PubMed]

43. Berndt, W. Iodine Adsorption on Silver (111) Studied by LEED. *Jpn. J. Appl. Phys.* **1974**, *13*, 653. [CrossRef]

44. Rastgoo-Lahrood, A.; Lischka, M.; Eichhorn, J.; Samanta, D.; Schmittel, M.; Heckl, W.M.; Lackinger, M. Reversible intercalation of iodine monolayers between on-surface synthesised covalent polyphenylene networks and Au(111). *Nanoscale* **2017**, *9*, 4995–5001. [CrossRef] [PubMed]

45. Moreno, C.; Vilas-Varela, M.; Kretz, B.; Garcia-Lekue, A.; Costache, M.V.; Paradinas, M.; Panighel, M.; Ceballos, G.; Valenzuela, S.O.; Peña, D.; et al. Bottom-up synthesis of multifunctional nanoporous graphene. *Science* **2018**, *360*, 199–203. [CrossRef]

46. Judd, C.J.; Junqueira, F.L.Q.; Haddow, S.L.; Champness, N.R.; Duncan, D.A.; Jones, R.G.; Saywell, A. Structural characterisation of molecular conformation and the incorporation of adatoms in an on-surface Ullmann-type reaction. *Commun. Chem.* **2020**, *3*, 166. [CrossRef]

47. Zhang, Z.; Perepichka, D.F.; Khaliullin, R.Z. Adatoms in the Surface-Confined Ullmann Coupling of Phenyl Groups. *J. Phys. Chem. Lett.* **2021**, *12*, 11061–11069. [CrossRef]

48. Fritton, M.; Duncan, D.A.; Deimel, P.S.; Rastgoo-Lahrood, A.; Allegretti, F.; Barth, J.V.; Heckl, W.M.; Björk, J.; Lackinger, M. The Role of Kinetics versus Thermodynamics in Surface-Assisted Ullmann Coupling on Gold and Silver Surfaces. *J. Am. Chem. Soc.* **2019**, *141*, 4824–48323. [CrossRef]

49. Nacci, C.; Schied, M.; Civita, D.; Magnano, E.; Nappini, S.; Píš, I.; Grill, L. Thermal- vs Light-Induced On-Surface Polymerization. *J. Phys. Chem. C* **2021**, *125*, 22554–22561. [CrossRef]

50. Song, W.; Martsinovich, N.; Heckl, W.M.; Lackinger, M. Thermodynamics of halogen bonded monolayer self-assembly at the liquid–solid interface. *Chem. Commun.* **2014**, *50*, 13465–13468. [CrossRef]

51. Gutzler, R.; Fu, C.; Dadvand, A.; Hua, Y.; MacLeod, J.M.; Rosei, F.; Perepichka, D.F. Halogen Bonds in 2d Supramolecular Self-Assembly of Organic Semiconductors. *Nanoscale* **2012**, *4*, 5965. [CrossRef]

52. Gatti, R.; MacLeod, J.M.; Lipton-Duffin, J.A.; Moiseev, A.G.; Perepichka, D.F.; Rosei, F. Substrate, Molecular Structure, and Solvent Effects in 2D Self-Assembly via Hydrogen and Halogen Bonding. *J. Phys. Chem. C* **2014**, *118*, 25505–25516. [CrossRef]

53. Teyssandier, J.; Mali, K.S.; De Feyter, S. Halogen Bonding in Two-Dimensional Crystal Engineering. *ChemistryOpen* **2020**, *9*, 225–241. [CrossRef] [PubMed]

54. Cavallo, G.; Metrangolo, P.; Milani, R.; Pilati, T.; Priimagi, A.; Resnati, G.; Terraneo, G. The Halogen Bond. *Chem. Rev.* **2016**, *116*, 2478–2601. [CrossRef] [PubMed]

55. Verzhbitskiy, I.A.; De Corato, M.; Ruini, A.; Molinari, E.; Narita, A.; Hu, Y.; Schwab, M.G.; Bruna, M.; Yoon, D.; Milana, S.; et al. Raman Fingerprints of Atomically Precise Graphene Nanoribbons. *Nano Lett.* **2016**, *16*, 3442–3447. [CrossRef]